

A Cellular Automata and a Partial Differential Equation Model of Tumor–Immune Dynamics and Chemotaxis

Andrea K. Cooper and Peter S. Kim

Abstract Immunotherapy is a newly emerging approach to cancer treatment that seeks to stimulate a body’s immune defenses, especially T cells, to combat and potentially eliminate tumors. Relevant tumor–immune interactions depend on stochasticity, since the dynamics involve a small and decreasing number of cells, and spatiotemporal heterogeneity, since the dynamics occur in a localized tumor environment. To account for these two aspects of the system, we develop mathematical models of an anti-tumor immune response using a cellular automaton and a system of partial differential equations. We explicitly model immune cell recruitment to the tumor via cytokine secretion and chemotaxis of immune cells. Our models exhibit three types of behavior: tumor elimination, oscillation, and uncontrolled tumor growth that depend substantially on the strength of immune cell chemotaxis, or recruitment, to the tumor site.

1 Introduction

The early stages of tumor growth are important to understand in medicine. It is the time when the tumor is most vulnerable, but also the least likely to be detected. A modern approach to combat tumor development is cancer vaccination [42]. Vaccination takes advantage of the immune system’s natural capacity to fight pathogens and is seen as an effective means of controlling infectious diseases. Now, researchers are attempting to use a similar technique in the treatment of cancer, and experimental evidence has repeatedly shown that the immune system is capable of selectively targeting tumor cells [21, 52, 53, 56]. However, the dynamics of the anti-tumor immune response remain poorly understood making it difficult to translate these results into effective clinical treatments [17, 49].

By developing mathematical and computational models, we can gain a better understanding of the dynamics of the system and help us determine which

A.K. Cooper • P.S. Kim (✉)

School of Mathematics and Statistics, University of Sydney, Camperdown, NSW 2006, Australia
e-mail: acoo9460@uni.sydney.edu.au; pkim@maths.usyd.edu.au

© Springer Science+Business Media New York 2014

A. Eladdadi et al. (eds.), *Mathematical Models of Tumor-Immune System Dynamics*, Springer Proceedings in Mathematics & Statistics 107,
DOI 10.1007/978-1-4939-1793-8_2

parameters most strongly influence the success or failure of an anti-tumor immune response. In this study, we are most interested in cytotoxic T lymphocytes, or effector T cells, since these are the immune agents that are most commonly stimulated by cancer vaccines and other immunotherapies [42]. Effector T cells interact with cells via a T cell receptor that binds to specific protein sequences, called antigens, and when an effector T cell interacts strongly enough, it kills the target cell [22]. Effector T cells that react to unique and specific antigens on tumor cells are called tumor-specific or anti-tumor effector T cells.

A variety of mathematical models have applied a range of modeling approaches to study tumor-immune interactions. Tumor-immune models have been formulated using ordinary differential equations (ODE) [1, 8, 23, 27, 29–32, 38, 40, 47], delay differential equations (DDE) [3, 4, 6, 11, 12, 26, 45, 55], partial differential equations (PDE) [14, 35, 36], impulsive differential equations [5], and fractional differential equations [15]. A recent review of tumor immune models using ODE systems can be found in [13]. Other papers develop agent-based models (ABM), cellular automata (CA), and hybrid formulations [25, 34, 46, 48].

In this chapter, we focus particularly on the hybrid CA-PDE model in Mallet and De Pillis [34] and the hybrid ABM-DDE model of Kim and Lee [25]. Inspired by these models, we formulate a simplified CA to model tumor cell and effector T cell interactions. Extending these two models, we add a chemoattractant population and incorporate the chemotaxis of effector cells up the gradient. During an immune response, effector cells recruit other effectors to the target site by secreting several immunostimulatory cytokines, such as IL-2 and IL-15, and chemokines, such as MIP-1 α [7, 33, 37, 61]. Experiments have also demonstrated that the same type of effector recruitment occurs during an effector response against a tumor [52, 53].

Neither [34] or [25] explicitly model effector recruitment via chemotaxis, both opting for a simplified, phenomenological approach. An important extension to these two models is to incorporate effector recruitment by chemotaxis, so that we can understand if chemotactic recruitment influences the effectiveness of an anti-tumor immune response. In this chapter, we discuss how we can develop a CA model and derive an analogous PDE model of tumor-effector interactions with chemotaxis.

The chapter is organized as follows: In Sect. 2, we present a probabilistic CA, in which tumor and effector cell motion and interactions are modeled probabilistically, while cytokine diffusion is modeled deterministically, and we show numerical simulations of the CA and discuss how chemotaxis influences the success or failure of the anti-tumor immune response. In Sect. 3, we show how to derive an analogous PDE model as a mean field approximation of the probabilistic CA, and we show numerical simulations of the PDE model and compare them to simulations of the CA. In Sect. 4, we discuss similarities and differences between the CA and PDE approaches and suggest possible directions for future work.

2 Individual Cell-Based Model

In this section, we develop a probabilistic CA model of tumor–immune interactions. For simplicity, we model the tumor–effector system on a two-dimensional plane as in [34], although it is straightforward to extend the system to three-dimensions as in [25]. As in [34], we consider a square domain $[-L, L] \times [-L, L]$, partitioned into square elements of width and height Δx .

We consider four populations: (1) tumor cells, (2) effector cells, (3) tumor–effector complexes, and (4) cytokines. At each time step of length Δt , these populations are updated according to probabilistic and deterministic rules described below.

Tumor Cells At each time step, each tumor cell attempts to divide with probability $1 - e^{-\Delta t/\tau_{\text{div}}}$, where τ_{div} is the average time between tumor cell divisions. When a tumor cell attempts to divide, it randomly chooses one of the four squares (up, down, left, or right) adjacent to its position with equal probability $1/4$. If that square does not already contain a tumor cell or a tumor–effector complex, a new tumor cell is placed there, representing a newly divided tumor cell. If a new tumor cell is placed in a square only occupied by an effector cell, they form a tumor–effector complex. We ignore any newly divided tumor cells that get placed outside the domain $[-L, L] \times [-L, L]$.

Effector Cells Effector cells migrate according to a random walk. At each time step of duration Δt , each effector cell tries to move one step of length Δx to one of the four adjacent squares, up, down, left, and right, with probabilities p_{up} , p_{down} , p_{left} , and p_{right} , respectively. The probabilities are functions of the cytokine concentrations at the effector’s location and four adjacent squares.

We devise our chemotaxis model using a weighted random walk. An effector at point (x, y) chooses to try to move one step up, down, left, or right with relative weightings

$$\begin{aligned} w_{\text{up}} &= 1 + \lambda C(x, y + \Delta x, t) , \\ w_{\text{down}} &= 1 + \lambda C(x, y - \Delta x, t) , \\ w_{\text{left}} &= 1 + \lambda C(x - \Delta x, y, t) , \\ w_{\text{right}} &= 1 + \lambda C(x + \Delta x, y, t) , \end{aligned} \tag{1}$$

for some nonnegative constant λ . See Fig. 1a.

As we see in (1), the relative weighting in each direction grows linearly with respect to the cytokine concentration in the corresponding square. The probabilities of moving in each direction are given by

$$p_{\text{up}} = \frac{w_{\text{up}}}{w_{\text{total}}}, \quad p_{\text{down}} = \frac{w_{\text{down}}}{w_{\text{total}}}, \quad p_{\text{left}} = \frac{w_{\text{left}}}{w_{\text{total}}}, \quad p_{\text{right}} = \frac{w_{\text{right}}}{w_{\text{total}}},$$

where $w_{\text{total}} = w_{\text{up}} + w_{\text{down}} + w_{\text{left}} + w_{\text{right}}$.

If an effector tries to move into a square already containing an effector cell or tumor–effector complex, it does not move, but stays still. On the other hand, if an effector cell tries to move into a square occupied by a tumor cell, it moves and the tumor and effector cells form a tumor–effector complex. See Fig. 1b,c.

We assume that effector cells exist at a constant average concentration E_0 (in terms of cells per area) outside the domain of the model. We calculate the probability that a single effector migrates into the domain during one time step in the following manner. Consider the rim of adjacent squares shown in Fig. 2 just beyond the domain. The total area of the rim is $4(2L\Delta x)$, so the expected number of effectors on the rim at any given time is $8E_0L\Delta x$. If we assume that the presence of effectors in the rim is governed by a Poisson process, the probability that there is at least one effector on the rim at the start of a time step is $1 - e^{-8E_0L\Delta x}$. (For simplicity, let us assume that $8E_0L\Delta x \ll 1$ and make the approximation that at most one effector is on the rim at any time.)

If an effector is on the rim, we assume it is not affected by the cytokine gradient in the domain, so it has an equal probability of 1/4 of moving in any direction, including into the domain. If an effector tries to enter the domain during the next time step, we randomly choose the entry location among the internal squares along the edge of the domain. All edge squares are chosen with equal probability, except corner squares, which are counted twice, since they can be entered from two directions. If an effector tries to enter a square that is already occupied by an effector or tumor–effector complex, it is blocked and does not enter.

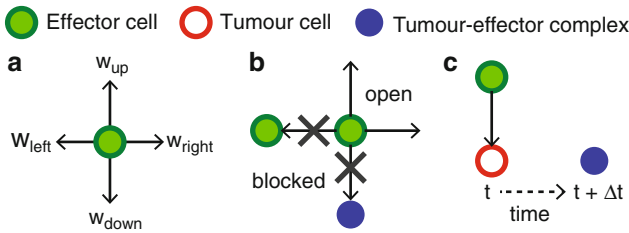


Fig. 1 Diagrams of rules of effector motion. (a) At each time step, an effector tries to move one step up, down, left, or right with relative weightings w_{up} , w_{down} , w_{left} , and w_{right} that depend on the cytokine concentrations in adjacent squares. (b) Effector cell motion is blocked if the space is occupied by an effector or tumor–effector complex. (c) If an effector tries to enter a space occupied by a tumor cell, the two cells form a tumor–effector complex

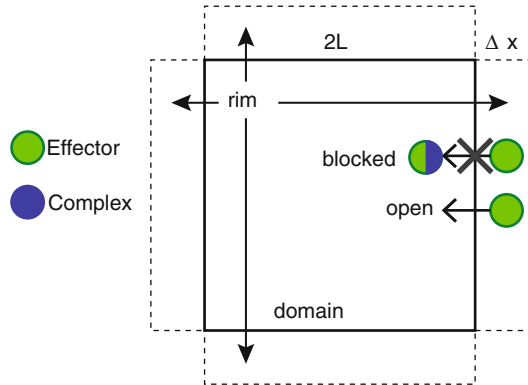
At each time step, effectors die with probability $1 - e^{-\Delta t/\tau_{\text{death}}}$, where τ_{death} is the average lifespan of effectors. As with tumor cells, if an effector migrates outside the domain $[-L, L] \times [-L, L]$, we eliminate it from the system.

Tumor–Effector Complexes Tumor–effector complexes form when tumor and effector cells end up in the same square. These complexes represent effectors engaging tumor cells. At each time step, we assume that the tumor cell in a complex dies with probability $1 - e^{-\Delta t/\tau_{\text{kill}}}$, where τ_{kill} is the average time for an effector to kill a tumor cell. In this case, the complex is replaced by only the effector.

Effectors in complexes can still die with probability $1 - e^{-\Delta t/\tau_{\text{death}}}$ at each time step. In this case, the complex is replaced by only the tumor cell. It is possible that both cells in a complex could die during the same time step, in which case the square is left empty.

Cytokine We assume that cytokine attracts effectors through chemotaxis and is secreted by effectors that are engaging tumor cells as tumor–effector complexes. This formulation is similar to the one in [34], which assumes that effectors interacting with tumor cells can induce, or recruit, other effectors into the region. Since our cytokines represent a huge number of molecules, we model the cytokine level in each square deterministically and continuously, rather than as a probabilistic collection of individual particles. The cytokine level at each square can be any nonnegative real number.

Fig. 2 Effector immigration into the domain. At each time step, an effector tries to enter the domain with probability $\frac{1}{4}(1 - e^{-8E_0L\Delta x})$. An entering effector has an equal chance of entering from any of the squares on the rim outside the domain. An effector cannot enter a square already occupied by an effector or tumor–effector complex



We assume cytokine levels decay exponentially at rate $1/\tau_{\text{ck}}$, are secreted by each tumor–effector complex at a constant rate σ , and diffuse with coefficient D_C . We estimate that cytokines diffuse approximately 20 times as fast as effectors [20], and we model cytokine diffusion deterministically, rather than as a random walk. Since the time scale of cytokine diffusion is much faster than other dynamics in the system, we assume that cytokine levels exist at quasi-steady state with respect to the locations of the tumor–effector complexes.

To calculate the quasi-steady state, we suppose a tumor–effector complex secretes cytokine as a point source centered at (x_0, y_0) . Then, using the fundamental solution of the diffusion equation [16], the steady-state cytokine level at (x, y) is given by

$$C(x, y) = \sigma \int_0^\infty \frac{1}{4\pi D_C t} \exp\left(-\frac{t}{\tau_{ck}}\right) \exp\left(-\frac{(x-x_0)^2 + (y-y_0)^2}{4D_C t}\right) dt. \quad (2)$$

We say that the cytokine level in a square of the CA grid is given by the expression $C(x, y)$ at the center of the square, so if a complex occupies a square centered at $(i\Delta x, j\Delta y)$, then the cytokine level at a square centered at $(k\Delta x, l\Delta y)$ is given by (2) for $x_0 = i\Delta x$, $y_0 = j\Delta y$, $x = k\Delta x$, and $y = l\Delta y$.

At every time step, we determine the quasi-steady state cytokine distribution of the entire system by determining the locations $(i_n\Delta x, j_n\Delta y)$ for $n = 1, \dots, N_X$ of all N_X complexes. Then, we evaluate (2) for each complex and sum the results to obtain the overall cytokine level in the CA.

Initial Conditions To initialize the simulation, we begin with one tumor cell at the center of the domain at $(0, 0)$ and iterate the system over several tumor cell divisions to obtain a starting tumor mass of between 150 and 250 cells around the center of the domain. As in [25, 34], we assume that the surrounding tissue plays a passive role, so we do not explicitly model it. All other populations begin at 0.

2.1 Parameter Estimates

We draw many of our parameter estimates from [25], which obtains its estimates from a variety of sources. Parameters, descriptions, and estimates are shown in Table 1.

Table 1 Parameters used in simulations of the cellular automaton

Parameter	Description	Estimate
Δt	Time step	1 min
Δx	Space step	12 μm
L	Half width of domain	606 μm
τ_{div}	Avg. time for tumor cell division	7 days = 10,080 min
τ_{death}	Avg. effector lifespan	2.5 day = 3,600 min
τ_{kill}	Avg. time for effector to kill tumor cell	1 day = 1,440 min
τ_{ck}	Avg. cytokine lifespan	1/2 day = 720 min
λ	Chemotaxis parameter in (1)	0, 60, or 120
σ	Secretion rate of cytokine by complexes	1/cell/min
E_0	Surrounding concentration of effectors	1×10^{-6} cells/ μm^2

Based on experimental results of Friedl and Gunzer and an estimate from Catron et al. we estimate that effectors migrate at velocity 12 $\mu\text{m}/\text{min}$ [9, 18], so for our time step, we set $\Delta t = 1$ min, and for the space step, we set $\Delta x = 12$ μm . This space step is convenient, because it is also approximately the diameter of a single cell [2, 9, 32, 34]. We assume that the domain of the CA is a grid with 101 squares on each side, so that the center square is located at $(0, 0)$. This means that the halfwidth of the grid is $L = 101\Delta x/2 = 606$ μm .

For consistency, we draw all of our experimental estimates of tumor growth rates from breast cancer data. Various experimental studies estimate tumor doubling times of approximately 1 month to a decade [28, 39, 54, 59]. Some mathematical models consider the possibility of aggressive early-stage tumors with division times of less than 10 days [27, 34]. In this chapter, we also model a fast-growing tumor with an average division time of $\tau_{\text{div}} = 7$ days as in [25]. This rate gives simulations that produce varied behavior more quickly.

During immune contraction, experiments have measured an effector half-life of 41 h [10], which corresponds to an average lifespan of $\tau_{\text{death}} = 41/\log(2)$ h = 2.5 days. We do not have clear estimates of the average times for effector killing of tumor cells, but experimental studies show that anti-tumor effectors can sometimes rapidly kill target cells and even kill multiple target cells simultaneously [60]. However, since the action of killing a target cell may require a long recovery period between consecutive killings, we use the conservative estimate of $\tau_{\text{kill}} = 1$ day, or an average of one per cell per day, as used in [25].

We do not have good estimates of cytokine decay rates, but we assume these molecules decay faster than the death rate of effector cells, so we estimate $\tau_{\text{ck}} = 1/2$ day. We also do not have good estimates of cytokine secretion rate, σ , by effector cells, but we observe that this parameter scales inversely with respect to λ . Indeed, if we multiply σ by a factor f , then we end up scaling the cytokine population, C , by a factor f , so if we scale λ by a factor $1/f$, the effectors act exactly the same. So, we only vary λ and keep σ fixed at 1 unit of cytokine per cell per minute. Based on experimentation, we choose the values 0, 60, and 120 for the chemotaxis parameter λ , because these values produce the three main dynamic behaviors of the system: uncontrolled tumor growth, oscillation, and rapid tumor elimination.

Since we are dealing with a two-dimensional CA, it is difficult to directly translate immune cell concentrations in units of cells per volume as used in [25] to units of cells per area. For our simulations, we choose an effector concentration of $E_0 = 1 \times 10^{-6}$ cells/ μm^2 , or 1 cell/ mm^2 .

2.2 Simulations of the Cellular Automata Model

We used Matlab R2011b to code and simulate the CA described in Sect. 2. Results of an example simulation are shown in Fig. 3. In this example, we use the parameters in Table 1 with chemotaxis parameter $\lambda = 120$.

Figure 3 shows the distribution of cells and cytokine levels for one simulation of the CA at time $t = 10$ days. There are 155 tumor cells, 5 effectors, and 15 tumor–effector complexes. The complexes secrete cytokine, causing a higher cytokine level in the vicinity of the tumor mass. Diffusion of cytokine produces a gradient that attracts circulating effectors towards the cluster of complexes surrounding the tumor mass.

Since the model is probabilistic, we run ten simulations to explore a range of probable behaviors. Effector cells eliminate the tumor population in all simulations. Figure 4 shows time evolutions of the fastest and slowest times to tumor elimination.

In Fig. 4a, effector cells find the tumor mass quickly, form tumor–effector complexes, and begin secreting cytokine, which attracts additional effectors, leading to rapid tumor elimination on day 31. The main difference in Fig. 4b is that effectors take longer to find the tumor, so the tumor grows to 421 cells before being eliminated on day 103. In all ten simulations, the ability of tumor–effector complexes to recruit additional effectors to the tumor site enables the immune response to eliminate the tumor population quickly.

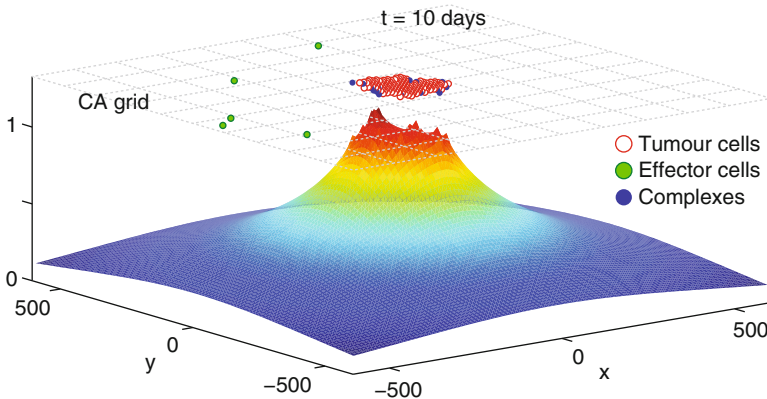


Fig. 3 Example CA simulation for chemotaxis parameter $\lambda = 120$ at time $t = 10$ days. Locations of tumor cells, effector cells, and tumor–effector complexes on the 2-D grid are shown at a height 10 % higher than the maximum cytokine level. Cytokine levels are shown by the surface plot. Other parameter values are taken from Table 1

To determine whether chemotaxis plays a role in the outcome of the anti-tumor immune response, we simulate the CA with chemotaxis parameter $\lambda = 0$, i.e., no chemotaxis. Figure 5 shows the state of the CA at time $t = 400$ days for one simulation.

In Fig. 5, the tumor has grown to 4,485 tumor cells on day 400. There are also 6 tumor–effector complexes and 1 effector. In contrast to the simulation shown in Fig. 3, tumor–effector complexes cannot recruit additional effectors, since effectors do not respond to the cytokine gradient. Without chemotaxis, the tumor–effector complexes are scattered around the tumor mass with hardly any clustering or aggregation of effectors or complexes (see Fig. 5). As a result, the effector response fails to control tumor growth. Figure 6 shows the time evolution of the cell populations for one simulation.

As we see in Fig. 6, the tumor population continues to grow at a steady rate without any surge in the effector response. All ten simulations that we ran using $\lambda = 0$ exhibit quantitatively similar behavior with the tumor population growing to between 3,980 and 4,634 cells by day 400. This result shows that chemotaxis of effectors plays a significant role in tumor elimination.

To see what happens for intermediate levels of chemotaxis, we run ten simulations of the CA with $\lambda = 60$. Results of an example simulation at time $t = 4,000$ days are shown in Fig. 7.

In Fig. 7, there are 1,154 tumor cells, 5 effectors, and 13 tumor–effector complexes on day 2,600. Unlike the case when $\lambda = 0$, the effector response has kept the tumor population under control even up to day 2,600. On the other hand, unlike the case when $\lambda = 120$, the effector response has not managed to eliminate the tumor by then. Nonetheless, as in the case when $\lambda = 120$, the effector response eventually succeeds in eliminating the tumor for all ten simulations, but the variability in time to elimination is much higher. Figure 8 shows time evolutions of the fastest and slowest times to tumor elimination.

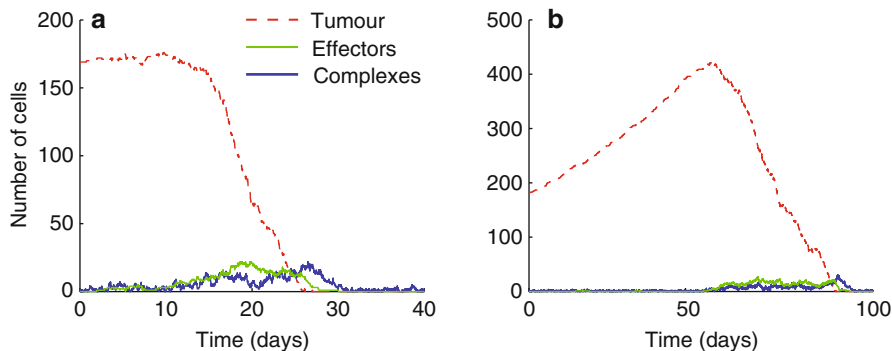


Fig. 4 Time evolution of tumor cells, effectors, and tumor–effector complexes when $\lambda = 120$. Other parameters values are taken from Table 1. (a) Fastest tumor elimination among ten simulations. Tumor is eliminated on day 31. (b) Slowest tumor elimination among ten simulations. Tumor is eliminated on day 103

Figure 8a shows that in the case when $\lambda = 60$, it is possible for effectors to eliminate the tumor without much of a relapse, but as shown in Fig. 8b, it is far more likely that the system oscillates. Oscillations occur because chemotaxis is strong enough to recruit a strong effector response against a large tumor; however, as the tumor shrinks to a smaller size, the number of tumor–effector complexes surrounding the tumor mass also declines, which reduces the amount of cytokine secreted at the tumor site. At this point the effector recruitment rate becomes too low to sustain the response against the tumor, and the tumor relapses.

The highly oscillatory scenario in Fig. 8b is most likely an undesirable outcome. The tumor reaches high peaks and does not get eliminated for a long time, so it is quite possible that tumor cells would have had time to mutate or metastasize, making it more difficult to treat.

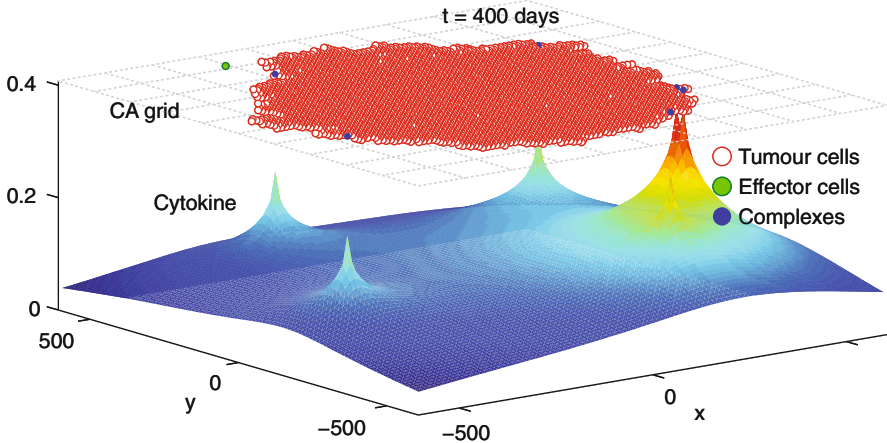
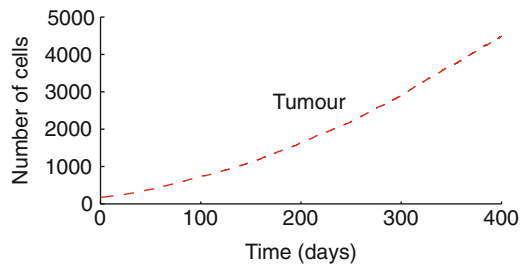


Fig. 5 Example CA simulation for chemotaxis parameter $\lambda = 0$, i.e., no chemotaxis, at time $t = 400$ days. Locations of tumor cells, effector cells, and tumor–effector complexes on the 2-D grid are shown at a height 10 % higher than the maximum cytokine level. Cytokine levels are shown by the surface plot. Other parameter values are taken from Table 1

Fig. 6 Time evolution of tumor cells. The effector response fails to control tumor growth, which reaches 4,485 cells on day 400. Numbers of effectors and complexes never exceed 6 and 7, respectively. Parameters values are taken from Table 1 with $\lambda = 0$



We have seen that the CA model exhibits a variety of behaviors and that chemotaxis of effectors plays a significant role in the final outcome. In the next section, we develop an analogous PDE model to see how a continuous, deterministic formulation of the system compares with the CA model.

3 Population Model

To investigate the system from the perspective of a deterministic dynamical system, we take a mean field approximation of the CA in Sect. 2 to obtain an analogous PDE model. The approach that we follow is similar to those of [44, 50, 51, 57, 58]. In fact, we directly use a result from Wang and Hillen [57], which we derive again here.

For simplicity, we show how we derive a mean field approximation in one space dimension. The generalization to higher dimensions is straightforward. Let us consider the following rules of cell motion (see Fig. 9):

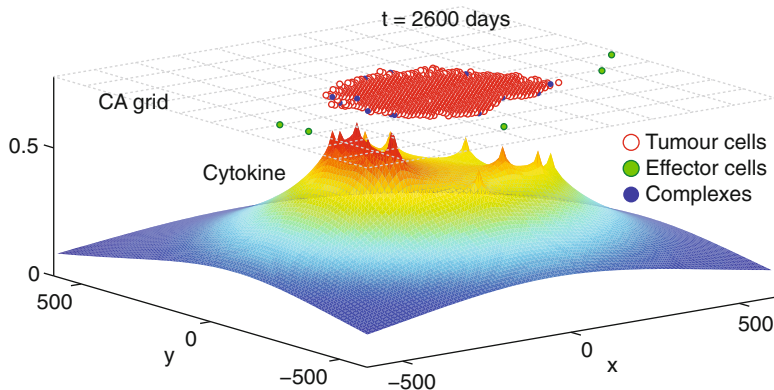


Fig. 7 Example CA simulation for chemotaxis parameter $\lambda = 60$ at time $t = 2,600$ days. Locations of tumor cells, effector cells, and tumor–effector complexes on the 2-D grid are shown at a height 10 % higher than the maximum cytokine level. Cytokine levels are shown by the surface plot. Other parameter values are taken from Table 1

1. At each time step Δt , a cell at point x tries to move left with probability $1/2 - \varepsilon(x, t)$ and right with probability $1/2 + \varepsilon(x, t)$.
2. A cell trying to enter point x succeeds in moving there with probability $q(x, t)$, called the *squeezing probability* in [57].

To derive our mean field model, we make the assumption that the number of individuals observed within any interval of space at any given time is independent of the number observed in any nonoverlapping interval [44, 50, 51, 57]. It is a standard assumption for mean field approximations and is sometimes called the *Poisson-point assumption* [43, p. 232].

Let $u(x, t)$ denote the density of cells at point (x, t) . To clean up notation, if $f = f(x, t)$ is a function of x and t , let us define $f_- = f(x - \Delta x, t)$ and $f_+ = f(x + \Delta x, t)$. Later on, when we take the limit to the continuum model, we also use f_x , f_{xx} , and f_t to denote the first and second partial derivatives of f with respect to x and the partial derivative of f with respect to t , respectively. From the rules of cell motion, also diagrammed in Fig. 9, we obtain the recursion

$$\begin{aligned}
 u(t + \Delta t) = & u - \left(\frac{1}{2} - \varepsilon\right) q_- u - \left(\frac{1}{2} + \varepsilon\right) q_+ u \\
 & + \left(\frac{1}{2} + \varepsilon_-\right) q u_- + \left(\frac{1}{2} - \varepsilon_+\right) q u_+ .
 \end{aligned} \tag{3}$$

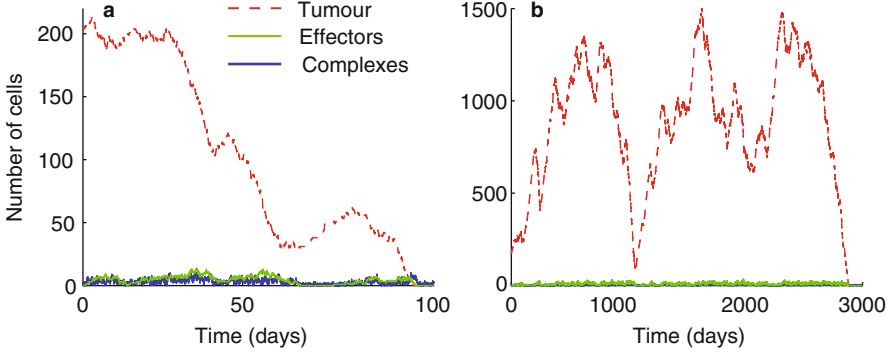


Fig. 8 Time evolution of tumor cells, effectors, and tumor–effector complexes when $\lambda = 60$. Other parameters values are taken from Table 1. **(a)** Fastest tumor elimination among ten simulations. Tumor is eliminated on day 105. **(b)** Slowest tumor elimination among ten simulations. The system is characterized by irregular, stochastic oscillations, and the tumor is eliminated on day 2,884

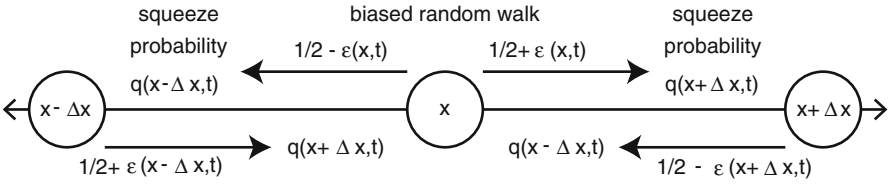


Fig. 9 Cell motion out of and into the point x . A cell at point x tries to move in a biased random walk with a right bias of $\varepsilon(x, t)$. If a cell tries to move to a point x , it successfully moves with squeeze probability $q(x, t)$

Simplifying (3), we obtain

$$\begin{aligned}
 u(t + \Delta t) - u &= \frac{1}{2} (-q_- u - q_+ u + q u_- + q u_+) + q_- \varepsilon u - q_+ \varepsilon u + q \varepsilon_- u_- - q \varepsilon_+ u_+ \\
 &= -\frac{q_- - 2q + q_+}{2} \cdot u + q \cdot \frac{u_- - 2u + u_+}{2} \\
 &\quad - (q_+ - q_-) \varepsilon u - q (\varepsilon_+ u_+ - \varepsilon_- u_-).
 \end{aligned}$$

After further rearrangement, we obtain

$$\begin{aligned}
 \frac{u(t + \Delta t) - u}{\Delta t} &= \left(\frac{\Delta x^2}{2 \Delta t} \right) \left[-\frac{q_- - 2q + q_+}{\Delta x^2} \cdot u + q \cdot \frac{u_- - 2u + u_+}{\Delta x^2} \right. \\
 &\quad \left. - \frac{4}{\Delta x} \left(\frac{q_+ - q_-}{2 \Delta x} \cdot \varepsilon u + q \cdot \frac{\varepsilon_+ u_+ - \varepsilon_- u_-}{2 \Delta x} \right) \right].
 \end{aligned}$$

Taylor expanding this expression, taking the limit as Δx and Δt go to zero, assuming that the random walk bias ε is of order Δx , so that the limit

$$E(x, t) = \lim_{\Delta x \rightarrow 0} \frac{\varepsilon(x, t)}{\Delta x}$$

exists, and assuming that the limit

$$D = \lim_{\substack{\Delta x \rightarrow 0 \\ \Delta t \rightarrow 0}} \frac{\Delta x^2}{2\Delta t}$$

exists, we arrive at the PDE

$$\begin{aligned} u_t &= D[-q_{xx}u + qu_{xx} - 4(q_x(Eu) + q(Eu)_x)] \\ &= D(qu_x - q_xu - 4qEu)_x . \end{aligned}$$

This derivation readily generalizes to the higher dimensional form

$$u_t = D\nabla \cdot (q\nabla u - u\nabla q - 4qEu) , \quad (4)$$

except that

$$D = \lim_{\substack{\Delta x \rightarrow 0 \\ \Delta t \rightarrow 0}} \frac{\Delta x^2}{4\Delta t} \quad \text{and} \quad D = \lim_{\substack{\Delta x \rightarrow 0 \\ \Delta t \rightarrow 0}} \frac{\Delta x^2}{6\Delta t} \quad (5)$$

for the 2-D and 3-D cases, respectively [41, 43].

For our particular model, consider the case of effectors, and for simplicity, let us consider 1-D random walks as before. The 1-D version of the random walk weightings (1) is given by

$$\begin{aligned} w_{\text{left}} &= 1 + \lambda C(x - \Delta x, y, t) , \\ w_{\text{right}} &= 1 + \lambda C(x + \Delta x, y, t) , \end{aligned}$$

and an effector moves right with probability

$$p_{\text{right}} = \frac{1 + \lambda C(x + \Delta x, y, t)}{2 + \lambda C(x - \Delta x, y, t) + \lambda C(x + \Delta x, y, t)} .$$

Taylor expanding this expression, we obtain

$$p_{\text{right}} = \frac{1}{2} + \frac{\lambda \Delta x}{2(1 + \lambda C)} C_x + o(\Delta x^3) ,$$

so the random walk bias is

$$\varepsilon(x, t) = \frac{\lambda \Delta x}{2(1 + \lambda C)} C_x + o(\Delta x^3),$$

which means that

$$E(x, t) = \lim_{\Delta x \rightarrow 0} \frac{\varepsilon(x, t)}{\Delta x} = \frac{\lambda \Delta x}{2(1 + \lambda C)} C_x.$$

Hence, we can rewrite (4) as

$$u_t = D \nabla \cdot (q \nabla u - u \nabla q - q \chi u \nabla v),$$

where

$$\chi(x, t) = \frac{2\lambda}{1 + \lambda C}, \quad v = C, \quad (6)$$

and it is straightforward to generalize this equation to higher dimensions. In general, our PDEs will be of the form

$$u_t = D \nabla \cdot (q \nabla u - u \nabla q - q \chi u \nabla v) + g(x, t) \quad (7)$$

for some growth function $g(x, t)$, which is also the form obtained in [57].

To obtain a PDE system based on the CA presented in Sect. 2, let the variables $T(\mathbf{r}, t)$, $E(\mathbf{r}, t)$, $X(\mathbf{r}, t)$, and $C(\mathbf{r}, t)$ denote the population densities at point \mathbf{r} and time t of tumor cells, effectors, complexes, and cytokine, respectively. A diagram of interactions is shown in Fig. 10.

Tumor Cells For the tumor population $T(\mathbf{r}, t)$, let us assume that tumor cells diffuse at some slow rate $D = D_T$ and grows logistically at rate $\rho T(1 - (T + X)/K)$, where ρ is the maximum growth rate and K is the maximum possible density of cells of the same type. Note that in the CA, tumor cells do not actually diffuse. Instead, dividing cells sprout off new cells in adjacent squares as long as empty squares are available. This process is tricky to capture using a reaction-diffusion equation, and it would probably require a free boundary formulation as in [19], so for simplicity, we model tumor growth as a diffusion and logistic growth process.

We assume that the rate of tumor–effector interactions follows the law of mass action, so that the interaction rate is of the form αET , where α is the mass-action coefficient. In the CA of Sect. 2, the formation of complexes happens immediately when tumors and effectors came into contact, so we set α to be relatively high. Also, effector cells in complexes die with mortality rate μ , causing the complex to return to a tumor-cell state at rate μX . Combining all the rates of growth and interactions, we obtain the reaction term $g = \rho T(1 - (T + X)/K) - \alpha ET + \mu X$.

For tumor diffusion, we assume that the squeeze probability is $q = 1 - (T + X)/K$, so that the probability of entering a space is the fraction of space remaining unoccupied by tumor cells and complexes. Tumor cells do not respond to the cytokine gradient, so for tumors, the chemotaxis factor $\chi = 0$. Substituting these values of D , q , χ , and g into (7), we have the equation

$$T_t = D_T \nabla \cdot \left(\left(1 - \frac{X}{K} \right) \nabla T + \frac{T}{K} \nabla X \right) + \rho T \left(1 - \frac{T + X}{K} \right) - \alpha ET + \mu X \quad (8)$$

for tumor cells.

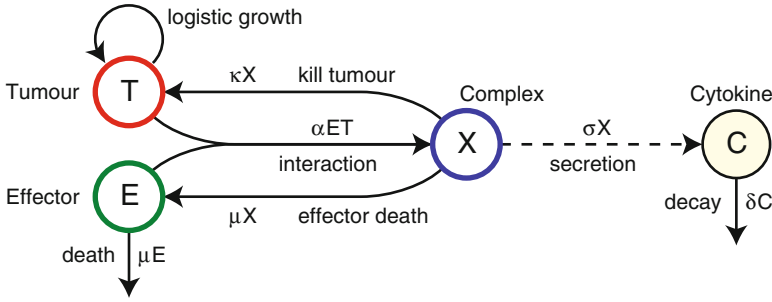


Fig. 10 Diagram of interactions for the PDE model. Tumor cells grow at a logistic rate $(1 - (T + X)/K)$. Effectors die at rate μE . Interacting tumors and effectors form complexes at rate αET . A complex reverts to a tumor cell or effector when the effector in the complex dies at rate μX or kills the tumor cell at rate κX , respectively. Complexes secrete cytokine at rate σX , and cytokine decays at rate δC . All cells diffuse and effector cells exist at a constant concentration at the boundary

Effector Cells For the effector population $E(\mathbf{r}, t)$, we have a diffusion rate $D = D_E$. Because effectors cannot move into spaces occupied by other effectors or complexes, the squeeze probability is $q = 1 - (E + X)/K$, where K is again the maximum density of cells of the same type. Effectors form complexes with tumor cells at rate αET , die at rate μE , and return from being part of a complex by killing the attached tumor cell at rate κX . We have the chemotaxis term χ from (6), so from (7), we obtain

$$E_t = D_E \nabla \cdot \left(\left(1 - \frac{X}{K} \right) \nabla E + \frac{E}{K} \nabla X - \left(1 - \frac{E + X}{K} \right) \frac{2\lambda E \nabla C}{1 + \lambda C} \right) - \alpha ET - \mu E + \kappa X. \quad (9)$$

Note that the chemotaxis term has a form that saturates as the cytokine concentration C grows. This form results from our rules of biased random motion of effectors in Sect. 2. As an alternative, if we replaced the relative weightings in (1) for motion in each direction by

$$\begin{aligned}
w_{\text{up}} &= 1 + \lambda(C(x, y + \Delta x, t) - C(x, y - \Delta x, t)) , \\
w_{\text{down}} &= 1 + \lambda(C(x, y - \Delta x, t) - C(x, y + \Delta x, t)) , \\
w_{\text{left}} &= 1 + \lambda(C(x - \Delta x, y, t) - C(x + \Delta x, y, t)) , \\
w_{\text{right}} &= 1 + \lambda(C(x + \Delta x, y, t) - C(x - \Delta x, y, t)) ,
\end{aligned}$$

and followed a similar derivation that we used to obtain (6), we would obtain a constant χ , which apart from the squeeze probability would correspond to the classical Keller–Segel model of chemotaxis [24].

Tumor–Effector Complexes We assume tumor–effector complexes $X(\mathbf{r}, t)$ diffuse at rate $D = D_T$, like tumor cells. Complexes cannot move into spaces occupied by either tumor cells or effectors, so their squeeze probability is $q = 1 - (T + E + X)/K$. Complexes form when tumor cells and effectors interact at rates αET , and they revert to single cells at rate $(\kappa + \mu)X$ when effectors kill the tumor cell or die. We assume that complexes do not respond chemotactically to the cytokine gradient. From (7), we obtain

$$X_t = D_T \nabla \cdot \left(\left(1 - \frac{E + T}{K} \right) \nabla X + \frac{X}{K} \nabla (E + T) \right) + \alpha ET - (\kappa + \mu)X. \quad (10)$$

Cytokine We assume cytokine $C(\mathbf{r}, t)$ diffuses at some rate $D = D_C$ without any volume exclusion, so that $q = 1$. Cytokine is secreted by complexes at rate σX and decays at rate δC , so from (7), we have

$$C_t = D_C \nabla^2 C + \sigma X - \delta C. \quad (11)$$

Boundary and Initial Conditions On the boundary of the domain, we assume that all populations have a constant value of 0, except the effector population, which has a constant density E_0 . For a simple initial condition, we assume that all populations start at 0 at time $t = 0$, except for the tumor population, which has value K on a disk of radius R , i.e., $T(\mathbf{r}, t) = \mathbf{1}_{\{\|\mathbf{r}\|^2 \leq R^2\}}$.

PDE System Combining (8)–(11), we have the system

$$\begin{aligned}
T_t &= D_T \nabla \cdot \left(\left(1 - \frac{X}{K} \right) \nabla T + \frac{T}{K} \nabla X \right) + \rho T \left(1 - \frac{T + X}{K} \right) - \alpha ET + \mu X , \\
E_t &= D_E \nabla \cdot \left(\left(1 - \frac{X}{K} \right) \nabla E + \frac{E}{K} \nabla X - \left(1 - \frac{E + X}{K} \right) \frac{2\lambda E \nabla C}{1 + \lambda C} \right) \\
&\quad - \alpha ET - \mu E + \kappa X , \\
X_t &= D_T \nabla \cdot \left(\left(1 - \frac{E + T}{K} \right) \nabla X + \frac{X}{K} \nabla (E + T) \right) + \alpha ET - (\kappa + \mu)X , \\
C_t &= D_C \nabla^2 C + \sigma X - \delta C .
\end{aligned}$$

This system can apply in any number of dimensions, but to keep in line with CA, we consider the system in two dimensions. However, since our model does not imply a favored spatial direction, we can reasonably assume that the system is radially symmetric and simplify the PDE system to one spatial dimension. If we assume radial symmetry and transform the system to polar coordinates, we obtain

$$\begin{aligned}
\frac{\partial T}{\partial t} &= D_T \frac{1}{r} \frac{\partial}{\partial r} \left[r \left(\left(1 - \frac{X}{K} \right) \frac{\partial T}{\partial r} + \frac{T}{K} \frac{\partial X}{\partial r} \right) \right] + \rho T \left(1 - \frac{T+X}{K} \right) - \alpha ET + \mu X, \\
\frac{\partial E}{\partial t} &= D_E \frac{1}{r} \frac{\partial}{\partial r} \left[r \left(\left(1 - \frac{X}{K} \right) \frac{\partial E}{\partial r} + \frac{E}{K} \frac{\partial X}{\partial r} - \left(1 - \frac{E+X}{K} \right) \frac{2\lambda E (\partial C / \partial r)}{1 + \lambda C} \right) \right] \\
&\quad - \alpha ET - \mu E + \kappa X, \\
\frac{\partial X}{\partial t} &= D_T \frac{1}{r} \frac{\partial}{\partial r} \left[r \left(\left(1 - \frac{E+T}{K} \right) \frac{\partial X}{\partial r} + \frac{X}{K} \frac{\partial (E+T)}{\partial r} \right) \right] + \alpha ET - (\kappa + \mu) X, \\
\frac{\partial C}{\partial t} &= D_C \frac{1}{r} \frac{\partial}{\partial r} \left[r \frac{\partial C}{\partial r} \right] + \sigma X - \delta C.
\end{aligned} \tag{12}$$

on domain $r \in (0, L)$ with boundary conditions $T(L, t) = 0$, $E(L, t) = E_0$, $X(L, t) = 0$, and $C(L, t) = 0$ with no-flux boundary conditions at $r = 0$. We also have the initial condition $T(r, t) = K$ for $r \leq R$ for some $R < L$ and $T(r, t) = 0$, otherwise. All other populations start at 0.

With the radially symmetric formulation (12), total populations are given by

$$P_{\text{tot}}(t) = 2\pi \int_0^L r P(r, t) dr$$

for all populations $P = T, E, X$, and C .

3.1 Parameter Estimates

We translate our parameters from values in Table 1 that we used for the CA in Sect. 2. A table of parameters, descriptions, and estimates are shown in Table 2.

We consider a domain of approximately the same size as with the CA, so we set the radius of the PDE domain to be $L = 600 \mu\text{m}$. In the CA, we allowed one cell to occupy a square of width $12 \mu\text{m}$, so our maximum density of cells of the same type is $K = 1 \text{ cell}/(12 \mu\text{m})^2 = 0.0069 \text{ cells}/\mu\text{m}^2$.

If we set the initial radius of the tumor to be $R = 100 \mu\text{m}$, this corresponds to an initial tumor population of $\pi R^2 K = 218$ cells, which is close to our initial condition for the CA of starting at around 200 cells.

In our past derivations, for simplicity, we obtained our PDEs from 1-D random walks, and so we used the relation that the diffusion rate of randomly walking cells is $\Delta x^2/(2\Delta t)$. These derivations generalize readily to higher dimensions, but in 2-D, the diffusion rate is given by $\Delta x^2/(4\Delta t)$ as in (5). Since our CA is built on a 2-D lattice, the effector diffusion rate that corresponds to a 2-D random walk of step size Δx and time step Δt is given by $D_E = \Delta x^2/(4\Delta t) = (12 \mu\text{m})^2/(2 \times 1 \text{ min}) = 36 \mu\text{m}^2/\text{min}$. We assume that the diffusion rate of tumor cells is very slow at $D_T = 0.0001 D_E$ and that the cytokine diffusion rate is twenty times the effector diffusion rate at $D_C = 20 D_E$, which agrees with the CA rules for cytokine diffusion in Sect. 2.

Table 2 Parameters used in simulations of the partial differential equation model

Parameter	Description	Unscaled estimate	Rescaled
L	Radius of domain	600 μm	0.6 mm
R	Radius of initial tumor	100 μm	0.1 mm
K	Maximum cell density	0.0069 cells/ μm^2	1 cell/ Δx^2
D_E	Diffusion rate of effector cells	36 $\mu\text{m}^2/\text{min}$	0.05 mm^2/day
D_T	Diffusion rate of tumor cells	0.0001 D_E	0.0001 D_E
D_C	Diffusion rate of cytokine cells	20 D_E	20 D_E
ρ	Logistic tumor growth rate	$9.9 \times 10^{-5}/\text{min}$	0.14/day
κ	Rate effectors kill tumor	$6.9 \times 10^{-4}/\text{min}$	1/day
μ	Mortality rate of effectors	$2.8 \times 10^{-4}/\text{min}$	0.4/day
σ	Secretion rate of cytokine	1/cell/min	1440 (cells/ Δx^2) $^{-1}$ day $^{-1}$
δ	Decay rate of cytokine	0.0014/min	2/day
α	Tumor–effector interaction rate	0.017/cell/min	24 (cells/ Δx^2) $^{-1}$ day $^{-1}$
λ	Chemotaxis parameter	0, 60, or 120	0, 60, or 120
E_0	Ambient effector concentration	1×10^{-6} cells/ μm^2	1.4×10^{-4} cells/ Δx^2

The tumor growth rate, effector killing rate, effector mortality rate, and cytokine decay rate are given by $\rho = 1/\tau_{\text{div}}$, $\kappa = 1/\tau_{\text{kill}}$, $\mu = 1/\tau_{\text{death}}$, and $\delta = 1/\tau_{\text{ck}}$, where parameters of the form τ are from Table 1. Values of the cytokine secretion rate σ , the cytokine parameter λ , and the ambient effector concentration rate E_0 can be used as is from Table 1.

We assume that the interaction rate between tumor cells and effectors in the same space is fast, so we set $\alpha = 24/\text{cell}/\text{day}$, which corresponds to an average interaction time of 1 h per cell. In column 3 of Table 2, we list all parameters in units of μm and minutes for consistency with the CA.

3.2 Rescaling of Parameters

Because the units in the third column of Table 2 have very disparate orders of magnitude, we rescale the system to time units of days and length units of millimeters and normalize the population such that the maximum density K scales to 1. As we will see, this rescaling will result in reasonable parameter values.

It is straightforward to rescale units of time and length to days and millimeters. Let K_0 denote the unscaled value of K , so that $K_0 = 6.9 \times 10^3$ cells/mm². The only other value that is affected by rescaling population densities is the ambient effector concentration, E_0 . The rescaled value of E_0 is E_0/K_0 . The rescaling puts all population densities in units of fraction of maximum cell density, or cells/ Δx^2 , where Δx is as in Table 1. Note that population units of cells⁻¹ in the CA translate without a conversion factor to population density units of (cells/ Δx^2)⁻¹ in the PDE, since one cell in the CA occupies an area of Δx^2 .

To calculate an unscaled value of a total population, we use

$$P_{\text{tot}}(t) = 2\pi K_0 \int_0^L rP(r,t)dr, \quad (13)$$

for populations $P = T, E, X$, and C , where the variable on the left-hand side is unscaled and the variable on the right-hand side is scaled.

3.3 Results of the Partial Differential Equation Model

We numerically simulate the PDE model (12) using the solver “pdepe” in Matlab R2011b. Figure 11 shows results of a numerical simulation using parameters in Table 2 with chemotaxis parameter $\lambda = 120$.

Figure 11a shows that the effector response causes a fast drop of the initial tumor population, resulting in a decline to 5.8 cells on day 41.8, which is comparable to the fastest time to tumor elimination for the CA shown in Fig. 4a. On the other hand, the effector response fades after the tumor reaches low levels, and the tumor relapses, leading to another effector response followed by a tumor decline in what appears to be an unstable oscillation. (Note that since we are dealing with a finite domain $r \in (0, L)$, the system will eventually approach an equilibrium in which the tumor population occupies nearly all of the domain, but we consider size of the domain somewhat arbitrary, since many tumors can expand to diameters of well beyond 1 mm before running into physical limitations.)

Figure 11b shows the profile of the tumor density, $T(r, t)$, at the six tumor peaks in Fig. 11a. As time progresses, each subsequent peak of tumor cells broadens and propagates farther from the origin. Since we are considering a radially symmetric system, the bulges in Fig. 11b correspond to rings of tumor cells around the origin. In contrast, in our simulations of the CA, we never saw a ring of tumor cells

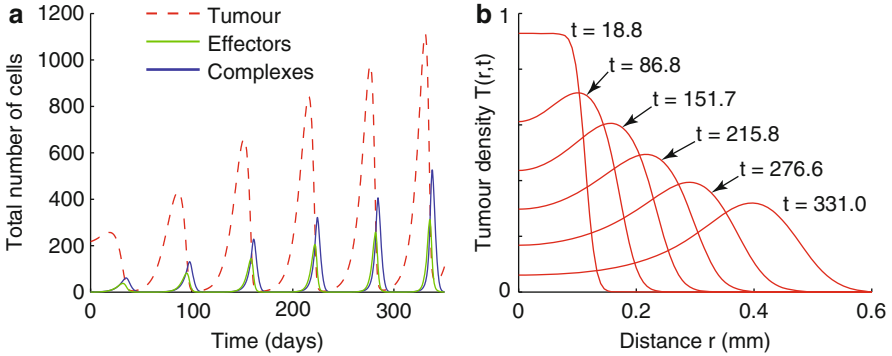


Fig. 11 Numerical solution of the PDE system (12) with chemotaxis parameter $\lambda = 120$. Other parameter values are taken from Table 2. (a) Time evolution of the total tumor, effector, and complex populations, calculated using (13). All three populations oscillate with six peaks between time 0 and 350. (b) Profile of tumor cell densities, $T(r, t)$, as a function of distance r from the origin at the times of the five tumor peaks at $t = 18.8, 86.8, 151.7, 215.8, 276.6$, and 331.0

propagating away from the origin even up to time 2,600 (see Fig. 7). Perhaps, this difference is due to the continuous nature of the PDE model versus the discrete nature of the CA. Incorporating a slow rate of tumor diffusion in the CA does not lead to a widening ring of relapsing tumor cells (data not shown), so slow tumor cell motion by itself is not enough to create a dispersing tumor. In any case, metastatic tumors are common, so it would be an interesting future direction to determine what dynamic characteristics of tumors would make tumor dispersal more likely. Examples of tumors that migrate away from a pursuing immune response occur in the model of Mallet and De Pillis [34].

To explore the system without chemotaxis, we consider the system when $\lambda = 0$ and plot the results in Fig. 12. As we found in the CA, the effector response in the PDE model without chemotaxis also cannot stop tumor growth (see Fig. 12a). Furthermore, the leading edge of the tumor population propagates with constant speed (see Fig. 12b). In fact, if we assume that the effector population remains so low as to be negligible, the equation for tumor growth simply reduces to Fisher's Equation.

We also consider the PDE model with $\lambda = 60$. Results of the numerical simulation are shown in Fig. 13. In this scenario, the effector response only manages to bring the tumor population down to 225.7 and 127.1 cells on days 213.1 and 287.6, respectively, and the magnitudes of the relapses increase more rapidly than in the case when $\lambda = 120$ (see Fig. 13a). As before, each successive relapse results in a ring of tumor cells that broadens and propagates away from the origin (see Fig. 13b).

As in Fig. 11a, the oscillations when $\lambda = 60$ also appear unstable. In contrast, none of the oscillations that we observed in simulations of the CA consistently grew in magnitude. Instead, the peak heights remained roughly the same until the effector response probabilistically eliminated the tumor (see Fig. 8b.)

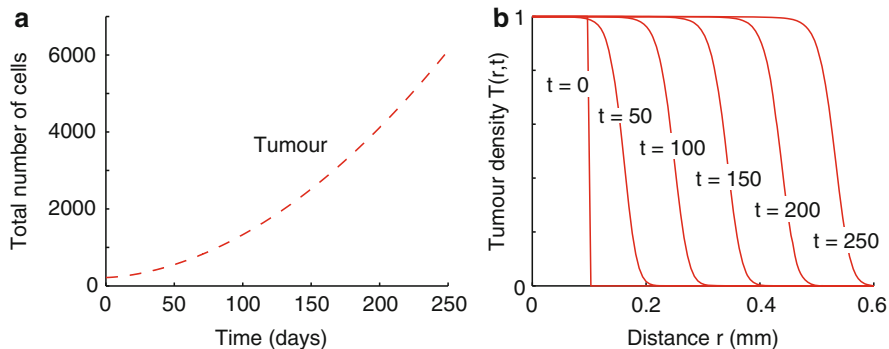


Fig. 12 Numerical solution of the PDE system (12) with chemotaxis parameter $\lambda = 0$. Other parameter values are taken from Table 2. (a) Time evolution of the total tumor population, calculated using (13). (b) Profile of tumor cell densities, $T(r, t)$ at $t = 0, 50, 100, 150,$ and 200

Like the CA, the PDE model is sensitive to the chemotaxis parameter λ , and higher λ leads to a stronger effector response against the tumor, while the absence of chemotaxis when $\lambda = 0$ leads to uncontrolled tumor growth. On the other hand, the PDE model behaves fundamentally differently from the CA model, because the PDE system does not result in complete elimination of the tumor population, and the unstable oscillations result in a widening ring of relapsing tumor cells traveling away from the origin, a phenomenon that we did not observe in our simulations of the CA. An interesting problem for future investigation would be to determine when the CA would exhibit fragmentation of a primary tumor mass into propagating secondary tumors.

4 Discussion

We develop a CA model of tumor and effector T cell interactions that is based on the hybrid CA-PDE model of Mallet and De Pillis [34] and agent-based model of Kim and Lee [25]; however, we explicitly add secretion of cytokines and chemotaxis to model immune recruitment. We then develop an analogous mean-field approximation of the CA as a system of PDEs and compare the PDE model to the CA.

For the CA, we see the three types of behavior also obtained in [25, 34]: rapid elimination of tumor, uncontrolled tumor growth, and a long period of oscillation before probabilistic tumor elimination. We obtained the three behaviors by only varying the chemotaxis parameter λ from relatively high sensitivity to chemoattractant at $\lambda = 120$ to no chemotaxis at $\lambda = 0$ and found that chemotaxis strongly influences the ability of the immune response to control or eliminate the tumor. These simulations corroborate the results of [25, 34], in which the authors find that T cell recruitment rates strongly influence the effectiveness of anti-tumor immune responses in both models.

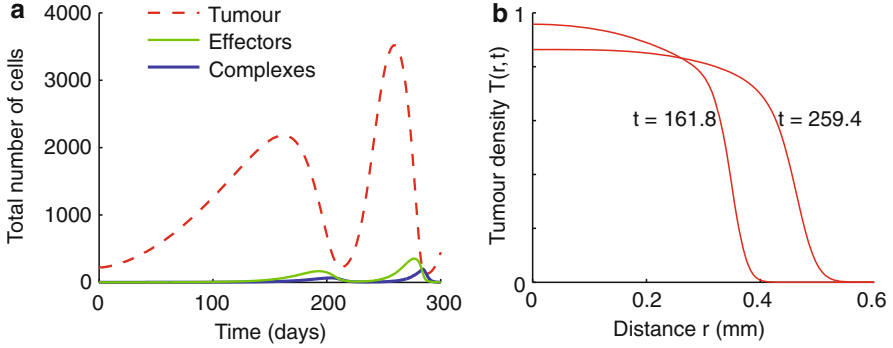


Fig. 13 Numerical solution of the PDE system (12) with chemotaxis parameter $\lambda = 60$. Other parameter values are taken from Table 2. (a) Time evolution of the total tumor, effector, and complex populations, calculated using (13). All three populations oscillate with two peaks between time 0 and 300. (b) Profile of tumor cell densities, $T(r, t)$, at the times of the tumor peaks at $t = 161.8$, and 259.4

Numerical simulations of the PDE model also show that dynamics are highly influenced by the chemotaxis parameter. For the parameter values in Table 2, which were chosen to be comparable to those of the CA, we do not see a stable solution corresponding to complete tumor elimination. In fact, it is possible that the underlying dynamics of the CA with strong chemotaxis is not stable either; it is just that effector recruitment is strong enough to ensure a high, but not guaranteed, chance of rapid tumor elimination (see Fig. 4a,b).

A direction for future work would be to determine under what conditions the PDE model is stable at the tumor-free equilibrium, produces oscillations, or leads to monotonic tumor growth. Both the PDE model and CA exhibit different characteristics making them useful to study independently and in comparison. The CA allows us to more realistically investigate stochasticity and variability of tumor growth, immune cell migration, and resulting outcomes. On the other hand, the PDE system can be numerically evaluated much faster than the CA and does not need to be evaluated multiple times to obtain the average behavior. Studying CA and PDE models in conjunction will also increase our understanding of the similarities and differences of modeling systems using discrete, probabilistic frameworks and continuous, deterministic models.

One could also conduct a more thorough parameter sensitivity analysis of the CA and PDE models of the same style done in [25]. As in [25], parameters that could be varied include the tumor growth rate, effector kill rate, sensitivity to cytokine gradients, and the ambient effector concentration. Such a parameter sensitivity analysis is relatively straightforward, but for the length and scope of this chapter, we do not delve into such a study here. In addition, it is also straightforward to convert the CA and PDE models to three dimensions as considered in [25].

Finally, the CA and PDE models in this chapter can be readily extended to devise even larger systems of tumor-immune dynamics that could include additional

populations, such as a heterogenous tumor population, additional immune cells, multiple cytokines, and chemotaxis of multiple cells to multiple signals. The role of CA and PDE models in cancer modeling will only grow in the coming years, and having an understanding of both modeling frameworks and connections between the two will become increasingly important in mathematical biology.

Acknowledgements AKC was supported by the KE Bullen Scholarship III awarded to honours students in the School of Mathematics and Statistics at the University of Sydney, and PSK was supported by the Australian Research Council Discovery Early Career Research Award (DE120101113).

References

1. Aguda, B.D., Marsh, C.B., Thacker, M., Crouser, E.D.: An in silico modeling approach to understanding the dynamics of sarcoidosis. *PLoS One* **6**(5), e19,544 (2011)
2. Alarcón, T., Byrne, H.M., Maini, P.K.: A cellular automaton model for tumour growth in inhomogeneous environment. *J. Theor. Biol.* **225**, 257–274 (2003)
3. Banerjee, S., Sarkar, R.R.: Delay-induced model for tumor-immune interaction and control of malignant tumor growth. *BioSystems* **91**(1), 268–288 (2008)
4. Barbarossa, M.V., Kuttler, C., Zinsl, J.: Delay equations modeling the effects of phase-specific drugs and immunotherapy on proliferating tumor cells. *Math. Biosci. Eng.* **9**(2), 241–257 (2012)
5. Bunimovich-Mendrazitsky, S., Byrne, H., Stone, L.: Mathematical model of pulsed immunotherapy for superficial bladder cancer. *Bull. Math. Biol.* **70**(7), 2055–2076 (2008)
6. Buzea, C.G., Agop, M., Moraru, E., Stana, B.A., Gir?u, M., Iancu, D.: Some implications of Scale Relativity theory in avascular stages of growth of solid tumors in the presence of an immune system response. *J. Theor. Biol.* **282**(1), 52–64 (2011)
7. Cabrero, J.R., Serrador, J.M., Barreiro, O., Mittelbrunn, M., Naranjo-Suarez, S., Martin-Cofreces, N., Vicente-Manzanares, M., Mazitschek, R., Bradner, J.E., Avila, J., Valenzuela-Fernandez, A., Sanchez-Madrid, F.: Lymphocyte chemotaxis is regulated by histone deacetylase 6, independently of its deacetylase activity. *Mol. Biol. Cell* **17**(8), 3435–3445 (2006)
8. Castiglione, F., Piccoli, B.: Cancer immunotherapy, mathematical modeling and optimal control. *J. Theor. Biol.* **247**(4), 723–732 (2007)
9. Catron, D.M., Itano, A.A., Pape, K.A., Mueller, D.L., Jenkins, M.K.: Visualizing the first 50 h of the primary immune response to a soluble antigen. *Immunity* **21**(3), 341–347 (2004)
10. De Boer, R.J., Homann, D., Perelson, A.S.: Different dynamics of CD4+ and CD8+ T cell responses during and after acute lymphocytic choriomeningitis virus infection. *J. Immunol.* **171**(8), 3928–3935 (2003)
11. DeConde, R., Kim, P.S., Levy, D., Lee, P.P.: Post-transplantation dynamics of the immune response to chronic myelogenous leukemia. *J. Theor. Biol.* **236**(1), 39–59 (2005)
12. Depillis, L., Gallegos, A., Radunskaya, A.: A model of dendritic cell therapy for melanoma. *Front. Oncol.* **3**, 56 (2013)
13. Eftimie, R., Bramson, J.L., Earn, D.J.: Interactions between the immune system and cancer: a brief review of non-spatial mathematical models. *Bull. Math. Biol.* **73**(1), 2–32 (2011)
14. Eikenberry, S., Thalhauser, C., Kuang, Y.: Tumor-immune interaction, surgical treatment, and cancer recurrence in a mathematical model of melanoma. *PLoS Comput. Biol.* **5**, e1000,362 (2009)

15. Erjaee, G.H., Ostadzad, M.H., Amanpour, S., Lankarani, K.B.: Dynamical analysis of the interaction between effector immune and cancer cells and optimal control of chemotherapy. *Nonlinear Dyn. Psychol. Life Sci.* **17**(4), 449–463 (2013)
16. Evans, L.C.: *Partial Differential Equations*, 2nd edn. American Mathematical Society, Providence (2010)
17. Finn, O.J.: Cancer vaccines: between the idea and the reality. *Nat. Rev. Immunol.* **3**, 630–641 (2003)
18. Friedl, P., Gunzer, M.: Interaction of T cells with APCs: the serial encounter model. *Trends Immunol.* **22**(2), 187–191 (2001)
19. Friedman, A., Tian, J.P., Fulci, G., Chiocca, E.A., Wang, J.: Glioma virotherapy: effects of innate immune suppression and increased viral replication capacity. *Cancer Res.* **66**(4), 2314–2319 (2006)
20. Goodhill, G.J.: Diffusion in axon guidance. *Eur. J. Neurosci.* **9**(7), 1414–1421 (1997)
21. Jaini, R., Kesaraju, P., Johnson, J.M., Altuntas, C.Z., Jane-Wit, D., Tuohy, V.K.: An autoimmune-mediated strategy for prophylactic breast cancer vaccination. *Nat. Med.* **16**, 799–803 (2010)
22. Janeway Jr., C.A., Travers, P., Walport, M., Shlomchik, M.J.: *Immunobiology : The Immune System in Health and Disease*, 6th edn. Garland Science Publishing, New York (2005)
23. Kareva, I., Berezovskaya, F., Castillo-Chavez, C.: Myeloid cells in tumour-immune interactions. *J. Biol. Dyn.* **4**(4), 315–327 (2010)
24. Keller, E.F., Segel, L.A.: Initiation of slime mold aggregation viewed as an instability. *J. Theor. Biol.* **26**, 399–415 (1970)
25. Kim, P.S., Lee, P.P.: Modeling protective anti-tumor immunity via preventative cancer vaccines using a hybrid agent-based and delay differential equation approach. *PLoS Comput. Biol.* **8**(10), e1002742 (2012)
26. Kim, P.S., Lee, P.P., Levy, D.: Dynamics and potential impact of the immune response to chronic myelogenous leukemia. *PLoS Comput. Biol.* **4**(6), e1000095 (2008)
27. Kirschner, D., Panetta, J.C.: Modeling immunotherapy of the tumor-immune interaction. *J. Math. Biol.* **37**, 235–252 (1998)
28. Kuroishi, T., Tominaga, S., Morimoto, T., Tashiro, H., Itoh, S., Watanabe, H., Fukuda, M., Ota, J., Horino, T., Ishida, T.: Tumor growth rate and prognosis of breast cancer mainly detected by mass screening. *Jpn. J. Cancer Res.* **81**(5), 454–462 (1990)
29. Kuznetsov, V.A., Makalkin, I.A., Taylor, M.A., Perelson, A.S.: Nonlinear dynamics of immunogenic tumors: parameter estimation and global bifurcation analysis. *Bull. Math. Biol.* **56**(2), 295–321 (1994)
30. León, K., Lage, A., Carneiro, J.: How regulatory CD25+CD4+ T cells impinge on tumor immunobiology? on the existence of two alternative dynamical classes of tumors. *J. Theor. Biol.* **247**(1), 122–137 (2007)
31. León, K., Lage, A., Carneiro, J.: How regulatory CD25+CD4+ T cells impinge on tumor immunobiology: the differential response of tumors to therapies. *J. Immunol.* **179**(9), 5659–5668 (2007)
32. Lin, A.: A model of tumor and lymphocyte interactions. *Discrete and Continuous Dynamical Systems B* **4**(1), 241–266 (2004)
33. Mackay, C.R.: Chemokine receptors and T cell chemotaxis. *J. Exp. Med.* **184**(3), 799–802 (1996)
34. Mallet, D.G., De Pillis, L.G.: A cellular automata model of tumor-immune system interactions. *J. Theor. Biol.* **239**, 334–350 (2006)
35. Matzavinos, A., Chaplain, M.A.: Travelling-wave analysis of a model of the immune response to cancer. *C. R. Biol.* **327**(11), 995–1008 (2004)
36. Matzavinos, A., Chaplain, M.A., Kuznetsov, V.A.: Mathematical modelling of the spatio-temporal response of cytotoxic T-lymphocytes to a solid tumour. *Math. Med. Biol.* **21**(1), 1–34 (2004)
37. Maurer, M., von Stebut, E.: Macrophage inflammatory protein-1. *Int. J. Biochem. Cell Biol.* **36**(10), 1882–1886 (2004)

38. Merrill, S.J.: A model of the role of natural killer cells in immune surveillance *I. J. Math. Biol.* **12**, 363–373 (1981)
39. Michaelson, J., Satija, S., Moore, R., Weber, G., Halpern, E., Garland, A., Kopans, D.B.: Estimates of breast cancer growth rate and sojourn time from screening database information. *J. Women Imaging* **5**(1), 11–19 (2003)
40. Moore, H., Li, N.K.: A mathematical model for chronic myelogenous leukemia (CML) and T cell interaction. *J. Theor. Biol.* **225**(4), 513–523 (2004)
41. Murray, J.D.: *Mathematical Biology: I. An Introduction*, 3rd edn. Springer, New York (2002)
42. Nestle, F.O., Tonel, G., Farkas, A.: Cancer vaccines: the next generation of tools to monitor the anticancer immune response. *PLoS Med.* **2**, e339 (2005)
43. Okubo, A., Levin, S.A.: *Diffusion and Ecological Problems: Modern Perspectives*, 2nd edn. Springer, New York (2010)
44. Penington, C.J., Hughes, B.D., Landman, K.A.: Building macroscale models from microscale probabilistic models: a general probabilistic approach for nonlinear diffusion and multispecies phenomena. *Phys. Rev. E* **84**(4 Pt 1), 041,120 (2011)
45. Pennisi, M.: A mathematical model of immune-system-melanoma competition. *Comput. Math. Methods Med.* **2012**, 850,754 (2012)
46. de Pillis, L.G., Mallet, D.G., Radunskaya, A.E.: Spatial tumor-immune modeling. *Comput. Math. Methods Med.* **7**(2–3), 159–176 (2006)
47. de Pillis, L.G., Radunskaya, A.E., Wiseman, C.L.: A validated mathematical model of cell-mediated immune response to tumor growth. *Cancer Res.* **65**(17), 7950–7958 (2005)
48. Qi, A.S., Zheng, X., Du, C.Y., An, B.S.: A cellular automaton model of cancerous growth. *J. Theor. Biol.* **161**(1), 1–12 (1993)
49. Robert-Tissot, C., Nguyen, L.T., Ohashi, P.S., Speiser, D.E.: Mobilizing and evaluating anticancer T cells: pitfalls and solutions. *Expert Rev. Vaccines* **12**(11), 1325–1340 (2013)
50. Simpson, M.J., Baker, R.E.: Corrected mean-field models for spatially dependent advection-diffusion-reaction phenomena. *Phys. Rev. E* **83**(5 Pt 1), 051,922 (2011)
51. Simpson, M.J., Landman, K.A., Hughes, B.D.: Multi-species simple exclusion processes. *Phys. A* **388**(4), 399–406 (2009)
52. Soiffer, R., Hodi, F.S., Haluska, F., Jung, K., Gillissen, S., Singer, S., Tanabe, K., Duda, R., Mentzer, S., Jaklitsch, M., Bueno, R., Clift, S., Hardy, S., Neuberger, D., Mulligan, R., Webb, L., Mihm, M., Dranoff, G.: Vaccination with irradiated, autologous melanoma cells engineered to secrete granulocyte-macrophage colony-stimulating factor by adenoviral-mediated gene transfer augments antitumor immunity in patients with metastatic melanoma. *J. Clin. Oncol.* **21**, 3343–3350 (2003)
53. Soiffer, R., Lynch, T., Mihm, M., Jung, K., Rhuda, C., Schmoltinger, J.C., Hodi, F.S., Lieber, L., Lam, P., Mentzer, S., Singer, S., Tanabe, K.K., Cosimi, A.B., Duda, R., Sober, A., Bhan, A., Daley, J., Neuberger, D., Parry, G., Rokovich, J., Richards, L., Drayer, J., Berns, A., Clift, S., Cohen, L.K., Mulligan, R.C., Dranoff, G.: Vaccination with irradiated autologous melanoma cells engineered to secrete human granulocyte-macrophage colony-stimulating factor generates potent antitumor immunity in patients with metastatic melanoma. *Proc. Natl. Acad. Sci. USA* **95**, 13,141–13,146 (1998)
54. Spratt, J.A., von Fournier, D., Spratt, J.S., Weber, E.E.: Decelerating growth and human breast cancer. *Cancer* **71**, 2013–2019 (1993)
55. Villasana, M., Radunskaya, A.: A delay differential equation model for tumor growth. *J. Math. Biol.* **47**(3), 270–294 (2003)
56. Wang, W., Epler, J., Salazar, L.G., Riddell, S.R.: Recognition of breast cancer cells by CD8+ cytotoxic T-cell clones specific for NY-BR-1. *Cancer Res.* **66**, 6826–6833 (2006)
57. Wang, Z., Hillen, T.: Classical solutions and pattern formation for a volume filling chemotaxis model. *Chaos* **17**(3), 037,108 (2007)
58. Wang, Z.A.: On chemotaxis models with cell population interactions. *Math. Model Nat. Phenom.* **5**(3), 173–190 (2010)
59. Weedon-Fekjaer, H., Lindqvist, B.H., Vatten, L.J., Aalen, O.O., Tretli, S.: Breast cancer tumor growth estimated through mammography screening data. *Breast Cancer Res.* **10**, R41 (2008)

60. Wiedemann, A., Depoil, D., Faroudi, M., Valitutti, S.: Cytotoxic T lymphocytes kill multiple targets simultaneously via spatiotemporal uncoupling of lytic and stimulatory synapses. *Proc. Natl. Acad. Sci. USA* **103**, 10,985–10,990 (2006)
61. Wilkinson, P.C., Komai-Koma, M., Newman, I.: Locomotion and chemotaxis of lymphocytes. *Autoimmunity* **26**(1), 55–72 (1997)